

Design, Synthesis, Spectral and Theoretical Studies of Some Picrates

S. AMALA¹, G. RAJARAJAN^{1,*}, E. DHINESHKUMAR¹, M. AROCKIA DOSS² and V. THANIKACHALAM¹

¹Department of Chemistry, Annamalai University, Annamalainagar-608002, India

²Department of Chemistry, St. Joseph University, Nagaland-797115, India

*Corresponding author: E-mail: rajarajang70@gmail.com

Received: 7 August 2019;

Accepted: 25 September 2019;

Published online: 18 November 2019;

AJC-19693

The structures of newly synthesized compounds (**1-3**) viz. 3-ethyl-5-methyl-2,6-bis(4-chlorophenyl)piperidin-1-ium picrate (**1**), 3-ethyl-5-methyl-2,6-bis(4-methylphenyl)piperidin-1-ium picrate (**2**) and 3-ethyl-5-methyl-2,6-bis(3,4-dimethoxyphenyl)piperidin-1-ium picrate (**3**) were confirmed by elemental analysis, FT-IR, ¹H and ¹³C NMR. The UV-visible spectra, fluorescence, emission properties of synthesized **1-3** in different solvents were studied. Compounds **1-3** solvatochromic displays a slight effect of the emission and absorption spectrum, indicating a small change in the dipole moment upon excitation of compounds **1-3**. All the compounds were investigated by DFT. The theoretical geometrical parameters are in good agreement with experimental values.

Keywords: Piperidin-1-ium picrate, Fluorescence, Density functional theory, Molecular electrostatic potential.

INTRODUCTION

Organic compounds have been extensively analyzed due to their non-linear optical (NLO) coefficient existing much larger than those of inorganic. Studies of molecular computational (DFT) can provide a deeper understanding of the relationship between molecular architecture, providing a range of optical properties [1-4]. Picric acid (2,4,6-trinitrophenol) is an organic compound used in the dyes industry and also as an explosive. This is a good π -acceptor for the neutral carrier donor molecule as there are three electron-withdrawing nitro groups [5,6]. On other hand, it also has an ability to form ionic bonds with picric acid and basic amino acids may also form charge-transfer complexes suitable for aromatic group with a dissociable [7,8]. These outstanding properties make them suitable for use in industrial processes in the chemical dye, leather and glass industry. Piperidin-4-one and its derivatives have undergone spectroscopic investigations in recent years because of a few examples of them its highly significant drug applications such as antiviral [9], antitumour [10], analgesic, local anesthetic [11,12], fungicidal, bactericidal and depressant drugs [13,14]. In the present study FT-IR, NMR and UV-visible and fluorescence spectral investigations of the compounds **1-3** have been performed using density functional theory (DFT). At first,

geometry optimization calculations were performed for B3LYP/6-31G (d,p) using the above method. The optimized structural parameters of the vibrational frequencies were used for stable conformer calculations. In addition, HOMO-LUMO Mulliken charge analysis and analysis of information have been used to support the structural properties. It has been calculated that various bonding electron densities (ED), redistribution motifs and E(2) energies in the natural bond orbital (NBO) provide analytical hyperlinking and originating from various intramolecular interactions [15]. The UV spectroscopic studies have been used along with HOMO-LUMO analysis to investigate the charge transfer within elucidate information [16]. The picrate anion easily forms π - π stacking and hydrogen bond interactions with antibodies to form an interesting 3D molecular structure. Meanwhile, in nitro group and π - π phase at a transition layer induction slip cycle can be obtained into the new organic switching dielectric. In recent years, much attention has been drawn to the incorporation of picric acid into organic conductors [17-20].

Considering that fourth-level phosphonium picrates inspired by this condition have not yet been discovered. We have shown the importance of positioning the electron donor-acceptor and chromophoric moieties onto the molecular frameworks for modulating the photophysical properties of piperidin

-4-one picrate, leading to efficient multicolour light emitting materials for organic electronics [21,22]. Owing to the interesting optical and photophysical properties of piperidin-4-one picrate, we tuned them by incorporating 3-pentyl-2,6-di(thiophen-2-yl)piperidin-4-one and picrate functionalities. New derivatives of 3-pentyl-2,6-di(thiophen-2-yl)piperidin-4-on-1-ium picrate were synthesized in high yields and purities for optical applications. Considering the prevailed literature this article reports a synthesis, molecular structure and investigation of electronic properties of compounds **1-3** with the assistance of DFT studies, were distributed and their electronic and non-linear properties were compared with similar derivatives accessible within the literature [23]. DFT calculation is a useful approach to scrutinize the coordinating interactions.

Arockia *et al.* [9] optimized the structures of the complexes of pentyl-2,6-di(furan-2-yl) piperidin-4-one by DFT calculation and the calculated structure of 3-ethyl-5-methyl-2,6-bis(4-chlorophenyl)piperidin-1-ium picrate was similar with present structure [24]. The successfully introduced three new synthetic biomolecular compounds, 3-ethyl-5-methyl-2,6-bis(4-chloro-phenyl)piperidin-1-ium picrate (**1**), 3-ethyl-5-methyl-2,6-bis(4-methylphenyl)piperidin-1-ium picrate (**2**), 3-ethyl-5-methyl-2,6-bis(3,4-dimethoxyphenyl)piperidin-1-ium picrate (**3**) characterized by FT-IR, CHN analysis, ^1H & ^{13}C NMR, UV-visible and fluorescence spectra. In addition, DFT investigations were performed on synthesized compounds in order to validate the experimental evidence.

EXPERIMENTAL

FT-IR spectra of the titled compounds were recorded in the region $4000\text{-}400\text{ cm}^{-1}$ using KBr pellet technique with 1.0 cm^{-1} resolution on AVATAR-330 FT-IR spectrometer. ^{13}C NMR spectra at 100 MHz and ^1H NMR spectra were recorded at 400 MHz on a BRUKER model using DMSO- d_6 as a solvent for all the compounds. Tetramethylsilane (TMS) was used as an internal reference for all NMR spectra, with chemical shifts reported in δ units (ppm) relative to the standard. Absorption spectral measurements were carried out with a UV 1650 PC model Shimadzu UV-visible spectrophotometer. Fluorescence spectra were recorded with a RF-5310PC Varian spectrofluorimeter using ethanol as solvent.

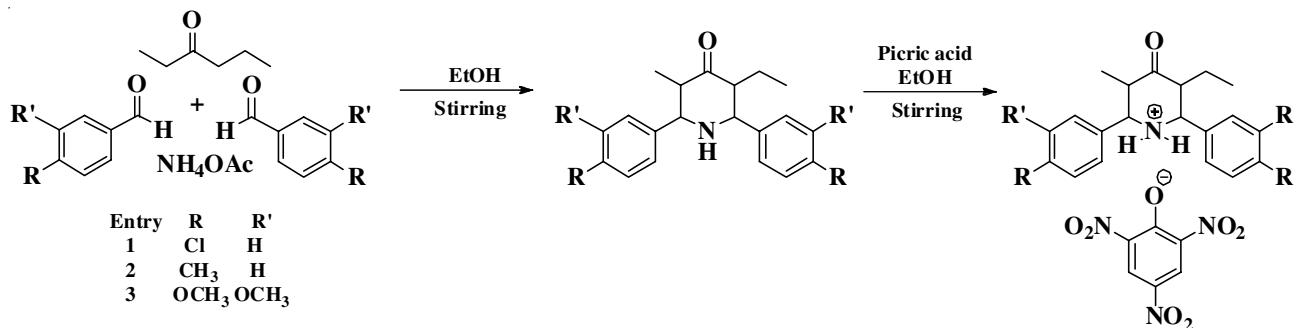
Synthesis of 3-ethyl-5-methyl-2,6-diarylpiperidin-1-ium picrate (1-3): In a 100 mL round bottom flask, 3-hexanone (1.0 equiv.), dry ammonium acetate (1.0 equiv.) and the appropriate aldehyde (2.0 equiv.) were dissolved in 50 mL ethanol. Subsequently, the reaction mixture was allowed to stir for 24 h

at ambient temperature under an air atmosphere. After 24 h, solvents were evaporated under vacuum and the precipitated 3-ethyl-5-methyl-2,6-diarylpiperidin-4-ones (**1-3**) residue was recrystallized from ethanol [15]. The equimolar solution of 3-ethyl-5-methyl-2,6-diarylpiperidin-4-one in ethanol and picric acid was stirred for 30 min. The yellowish solid formed was filtered. The obtained product was recrystallized to get excellent yield (**Scheme-I**).

3-Ethyl-5-methyl-2,6-bis(4-chlorophenyl)piperidin-1-ium picrate (1): Yield: 90 %; m.p.: 176-181 °C; Elemental analysis of $\text{C}_{26}\text{H}_{24}\text{N}_4\text{O}_8\text{Cl}_2$ calcd. (found) (%): C, 52.80 (52.71); H, 4.09 (4.00); N, 11.99 (12.99). IR (KBr, cm^{-1}): 3416 $\nu(\text{N-H})$, 3076 $\nu(\text{Ar-CH})$, 2987 $\nu(\text{ali.-CH})$, 1718 $\nu(\text{C=O})$, 1611 $\nu(\text{C=C})$, 1585, 1516, 1449 $\nu_{\text{asym}}(\text{NO}_2)$, 1372, 1335, 1234 $\nu_{\text{sym}}(\text{NO}_2)$, 1159 $\nu(\text{C-O})$, 1011, 833 $\beta_{\text{ar}}(\text{C-H})$, 766-724 $\tau_{\text{ar}}(\text{C-H})$. ^1H NMR (400 MHz, DMSO- d_6 , δ , ppm): 10.89 (s, eq-NH), 10.05 (s, ax-NH), 8.58 (s, 2H, picryl ring), 7.28-7.92 (m, 8H, Ar-H), 4.68 (1H, H_6), 4.59 (1H, H_2), 3.70 (1H, H H_{5a}), 3.47 (1H, H_{3a}), 1.2'-1.35 (m, 2H, CH_2), 0.73 (m, 6H, CH_3). ^{13}C NMR (100 MHz, DMSO- d_6 , δ , ppm): 204.35 (C=O), 160.79 (C-O), 124.37, 125.23, 128.48-134.24, 141.75 (Ar-C), 63.86 C(2), 62.44 C(6), 51.44 C(3), 46.17 C(5), 17.78 ($-\text{CH}_2-$), 10.79 (CH_3).

3-Ethyl-5-methyl-2,6-bis(4-methylphenyl)piperidin-1-ium picrate (2): Yield: 85 %; m.p.: 158-163 °C; Elemental analysis of $\text{C}_{28}\text{H}_{30}\text{N}_4\text{O}_8$ calcd. (found) (%): C, 61.08 (61.21); H, 5.49 (5.60); N, 10.18 (10.13). IR (KBr, cm^{-1}): 3428 (N-H *str.*), 3082 $\nu(\text{Ar-CH})$, 2934 $\nu(\text{ali.-CH})$, 1712 $\nu(\text{C=O})$, 1627 $\nu(\text{C=C})$, 1556, 1491, 1441, $\nu_{\text{asym}}(\text{NO}_2)$, 1366, 1313, 1273 $\nu_{\text{sym}}(\text{NO}_2)$, 1161 $\nu(\text{C-O})$, 1078, 938, 908 $\beta_{\text{ar}}(\text{C-H})$, 811, 784, 742 $\tau_{\text{ar}}(\text{C-H})$. ^1H NMR (400 MHz, DMSO- d_6 , δ , ppm): 9.99 (s, eq-NH), 9.54 (s, ax-NH), 8.58 (s, 2H, picryl ring), 7.00-7.28 (m, 8H, Ar-H), 4.60 (1H, H_6), 4.52 (1H, H_2), 3.24 (1H, H H_{5a}), 3.48 (1H, H_{3a}), 2.31 (Ar- CH_3), 1.21-1.35 (m, 2H, CH_2), 0.74 (m, 6H, CH_3). ^{13}C NMR (100 MHz, DMSO- d_6 , δ , ppm): 204.80 (C=O), 160.79 (C-O), 124.34, 125.21, 128.71-131.15, 139.16, 141.75, (Ar-C), 64.15 C(2), 62.73 C(6), 51.42 C(3), 46.15 C(5), 17.83 ($-\text{CH}_2-$), 20.71 (Ar- CH_3); 10.69 (CH_3).

3-Ethyl-5-methyl-2,6-bis(3,4-dimethoxyphenyl)piperidin-1-ium picrate (3): Yield: 70 %; m.p.: 162-167 °C; Elemental analysis of $\text{C}_{31}\text{H}_{36}\text{N}_4\text{O}_{12}$ calcd. (found) (%): C, 56.70 (56.56); H, 5.53 (5.23); N, 8.53 (8.53); IR (KBr, cm^{-1}): 3414 $\nu(\text{N-H})$, 3082 $\nu(\text{Ar-CH})$, 2983 $\nu(\text{ali.-CH})$, 1718 $\nu(\text{C=O})$, 1625 $\nu(\text{C=C})$, 1556, 1514, 1487 $\nu_{\text{asym}}(\text{NO}_2)$, 1429, 1358, 1265 $\nu_{\text{sym}}(\text{NO}_2)$, 1159 $\nu(\text{C-O})$, 1080 (C-N *str.*), 1028, 997, 808 $\beta_{\text{ar}}(\text{C-H})$, 707 $\tau_{\text{ar}}(\text{C-H})$. ^1H NMR (400 MHz, DMSO- d_6 , δ , ppm): 10.02 (s, eq-NH), 9.21(s, ax-NH), 8.65 (s, 2H, picryl ring), 7.11-7.22



Scheme-I: Synthetic route of compounds 1-3

(m, 8H, Ar-H), 4.61 (1H, H₆), 4.52 (1H, H₂), 3.51 (1H, H, H_{5a}), 3.21 (1H, H_{3a}), 2.56 (Ar-OCH₃); 1.30-1.48 (m, 2H, CH₂), 0.86 (m, 6H, CH₃). ¹³C NMR (100 MHz, DMSO-*d*₆, δ, ppm): 204.85 (C=O), 160.83 (C-O), 111.51, 112.15, 121.27-149.59 (Ar-C), 64.19 C(2), 62.77 C(6), 51.53 C(3), 46.25 C(5), 55.63, 55.48 (Ar-OCH₃); 17.91 (-CH₂-), 10.85 (CH₃).

Computational studies: The DFT calculations were performed on B3LYP with basis set 6-31G (d, p). The Cartesian representation of the compounds **1-3** in the geometry of tight convergence criterion under a fully optimized in-ground electronic state [19,25]. However, the most optimized structural parameters such as bond angle and length were obtained from Gaussian 03W. Mulliken partial charges in the molecule using Atomic analysis were obtained, similarly frontier molecular orbitals (FMO) [26,27], Mulliken charge of atoms [28,29], electrophilicity [30] of systems were also calculated. Calculations NBO [31] were performed to know the orbitals of the interactions between sub-systems, which denote a measure of the intramolecular delocalization. The electrophilic and nucleophilic regions were identified by MEP [32] using Gauss View 3.0. Moreover, many other parameters like molecular dipole moment, polarizability and first-order hyperpolarizability for the present compounds have been also presented. All calculations were performed on a personal computer by using the Gaussian 03W program package.

RESULTS AND DISCUSSION

FT-IR analysis: In the IR spectra of synthesized compounds **1-3**, amide >C=O stretching bands are observed at 1657-1639 cm⁻¹ in addition to ring carbonyl stretching band at 1720-1705 cm⁻¹. In the IR spectrum of compound **1**, NH stretching vibration is found at 3415 cm⁻¹ and theoretical results are found at 3416 cm⁻¹. The benzene derivatives of C-H stretching vibration appeared in the region 3100-3000 cm⁻¹ [33]. Accordingly, in the present investigation for compound **1**, the C-H symmetric stretching vibrations were observed at 3091, 3082 and 3073 cm⁻¹ in the theoretical FT-IR spectrum and 3076 cm⁻¹ are found in the experimental FT-IR spectrum. The asymmetric stretching vibrations were observed at 3073, 3055, 3046 and 3037 cm⁻¹ (theoretical) and 3045 cm⁻¹ (experimental). The absorption bands for C-C stretching modes occurred in the range of 1650-1200 cm⁻¹ for aromatic compounds [34,35]. For compound **3**, the bands were observed at 1585 and 1516 cm⁻¹ for experimental FT-IR spectrum. In addition, theoretical results happen at 1855, 1552 and 1543 cm⁻¹ for C-C stretching vibration. Experimental -C=N- and -NH stretching bands appeared at 1611 cm⁻¹ and theoretical ones were at 1615 cm⁻¹. For compound **3**, the strong two bands at 1449 and 1335 cm⁻¹ (experimental) and 1516 cm⁻¹ (theoretical) belongs to N-O stretching modes. The NO₂ asymmetric stretching vibrations of picryl moiety are observed at about 1451 cm⁻¹. In addition, experimental bands at 1449, 1335 and 1234 cm⁻¹ were due to NO₂ symmetric stret-

ching vibrations and theoretical results were found at 1498, 1327 and 1228 cm⁻¹. The bands at 912, 833 and 766 cm⁻¹ were due to the aromatic C-H out of plane bending vibrations for FT-IR spectrum.

NMR analysis: The ¹H NMR and ¹³C have been experimentally and theoretically executed to know the reaction rate of the molecule. The sharp signal at 8.6 ppm is due to the presence of two protons in the picryl ring. Introduction of substituent at phenyl ring in piperidones picryl ring signal does not affect. The aromatic proton signal observed in the interval of 7.00-7.28 ppm. In compound **2**, it had eight hydrogen atoms attached to carbon atoms in the aromatic ring. The ¹H experimental chemical shift of hydrogen atoms (*i.e.* H₆, H₂, H_{5a} and H_{3a}) occurred at 4.60, 4.52, 3.24, 3.48 ppm, respectively. In 6-halogen substituted chloride and methyl, dimethoxy molecules, it has five hydrogen atoms are attached to carbon atoms in the ring. The upfield signals in the region 1.21-1.35 ppm are attributed to methylene protons of ethyl group at C-3 and CH₃ group at C-5. The triplet signal at 0.74 ppm is observed for methyl proton of an ethyl group at C-3 in piperidin-4-one ring. Similar splitting patterns were observed for compounds **1** and **3**.

In the ¹³C NMR spectrum of compound **2**, methyl carbon of tolyl group gives a signal at 10.69 ppm. The sixteen aromatic carbons of phenyl and tolyl group appeared as multiplet in the range of 124.34, 125.21 and 128.71-139.16 ppm. In the present study, a signal found in ¹³C NMR spectrum at 163.73 ppm is because the carbon atoms belong to benzene ring, which had no binding. The signal at 147.75 ppm is assigned to C8 carbon of phenyl ring which is bonded with the NH group, calculated as 131.15 ppm. The most downfield signal at 204.80 ppm is obviously due to carbonyl carbon *i.e.* C-4. The shifting of signal towards downfield is due to neighbouring electronegative oxygen (O4) [36]. The upfield signal at 64.15 ppm is due to methine carbons *i.e.* C-2 and C-4. Among the remaining signals, the downfield signal is 46.15 ppm apparently due to C-1 and C-5, which are chemically equivalent [15]. The predicted chemical conversion values are in good agreement with the experimental values.

Solvent effect on absorption and emission spectra of compounds 1-3: Figs. 1 and 2 show the absorption and emission spectra of compounds **1-3** solutions (1 × 10⁻⁵ mol dm⁻³) measured in solvents of different polarity. The corresponding spectral data are summarized in Table-1. As indicated in Table-1, the solvent polarity shows a slight effect on the positions of the electronic absorption and emission maxima (*ca.* 10 nm). This effect could be due to the small polarity change in both the ground and excited states of the solvated **1-3**. The fluorescence quantum yield (φ_f) of compounds **1-3** is slightly affected by solvent polarity. Aromatic compounds that contain heteroatoms like nitrogen and oxygen often have low-lying, closely spaced π-π* and n-π* states. Inversion of these two states can be observed when the polarity and the hydrogen-bonding power

TABLE-1
ABSORBANCE AND EMISSION VALUES (WAVELENGTH, nm) OF COMPOUNDS 1-3

Solvent	Compound 1		Compound 2		Compound 3	
	Absorbance	Fluorescence	Absorbance	Fluorescence	Absorbance	Fluorescence
Chloroform	353	445	356	451	355	446
Methanol	347	449	351	452	349	448

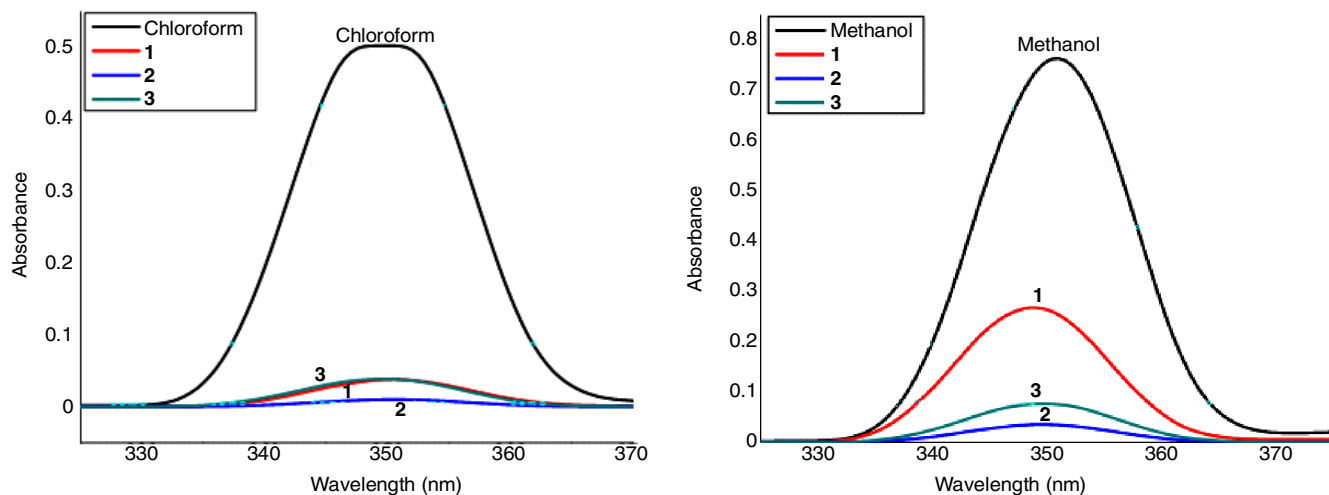


Fig. 1. Absorption spectra of compounds 1-3 with chloroform and methanol

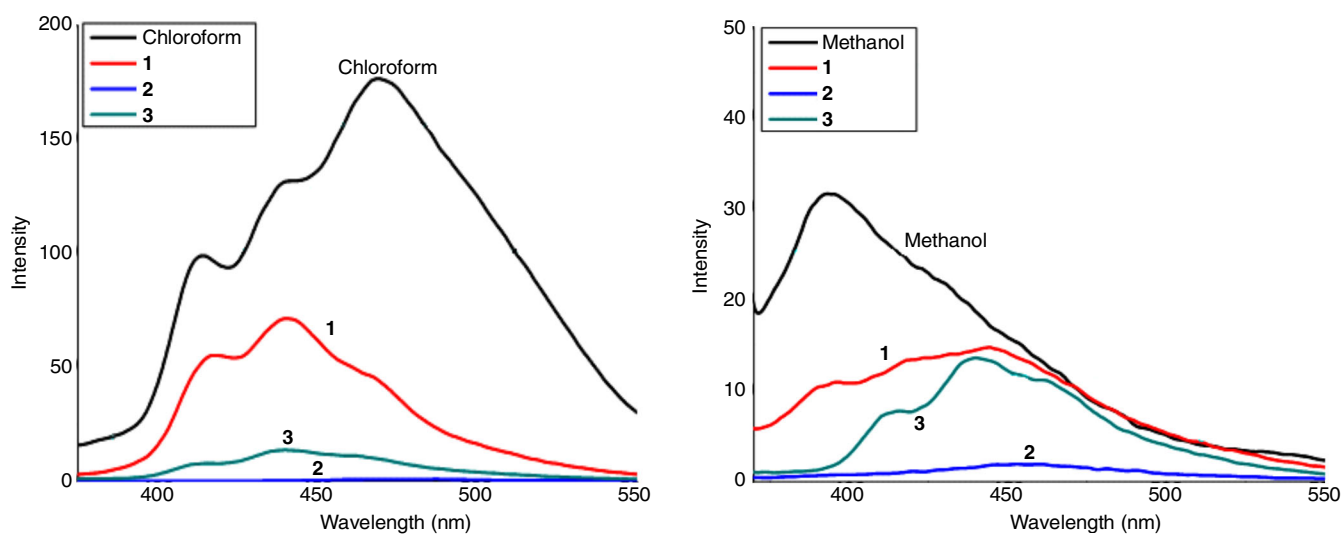


Fig. 2. Emission spectra of compounds 1-3 in chloroform and methanol

of the solvent increase. This is because of $n-\pi^*$ state shifts to higher energy whereas the $\pi-\pi^*$ shifts to lower energy. The outcome of this effect increases the fluorescence quantum yield because the radiative emission from $n-\pi^*$ state is known to be less efficient than that from the $\pi-\pi^*$ state.

Molecular geometry: The atom numbering scheme with the molecular structure of compounds (1-3) is given in Fig. 3. All the parameters allowed relaxation and all the calculations converged to an optimized geometry which corresponds to a true energy minimum as measured by the calculated vibrational

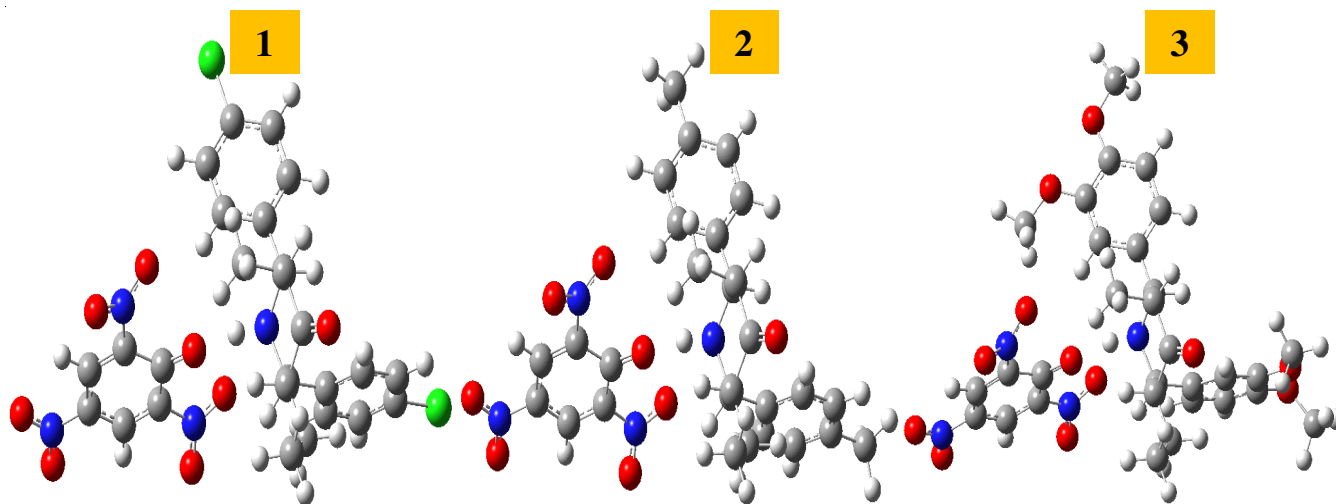


Fig. 3. Optimized structure of compounds 1-3

frequencies [37]. The optimized geometrical parameters are compared with the crystal structure of 3-pentyl-2,6-di(furan-2-yl)piperidin-4-one. Experimental values with B3LYP/6-31G(d,p) nearly coincides in the range of 1.554-1.516 Å in piperidine ring in the calculated C-C bond distance [9]. Literature value for C-H bond distance is found to be 1 Å.

The computed bond length lies between 1.104-1.089 Å for the heterocyclic ring. As seen in Table-2, the calculated bond length N1-H1A is 1.022 (B3LYP) Å which differs from the literature value (0.867 Å). The C3-C2-C11 and N1-C2-N11 angles are found to be 119.1 and 110.2°. The current bond angle of the nitro group in the picrate analogue dominates. This has been known in previous studies [9].

TABLE-2
SELECTED BOND LENGTHS (Å) OF COMPOUNDS 1-3

Bond	Compound 1	Compound 2	Compound 3
N1-C2	1.526	1.527	1.527
N1-H1A	1.022	1.022	1.022
N1-H1B	1.073	1.067	1.063
C2-C3	1.548	1.548	1.549
C3-C4	1.530	1.530	1.531
C4-C5	1.532	1.532	1.531
C4-O4	1.216	1.216	1.217
C5-C6	1.554	1.553	1.554
N1-C6	1.509	1.510	1.511
C3-C7	1.536	1.536	1.536
C2-C11	1.519	1.610	1.518
C6-C17	1.516	1.515	1.513
C23-O32	1.263	1.260	1.259
C23-C24	1.455	1.456	1.456
C23-C28	1.452	1.454	1.389
C24-C25	1.390	1.389	1.389
C28-C27	1.377	1.454	1.377
C26-C27	1.397	1.398	1.397
C26-C25	1.386	1.386	1.386

The results presented in Table-3 showed that piperidone ring essentially adopts chair conformation and also it is evident from the torsional angles N1-C2-C3-C4 (-52.4 and -59.5° at B3LYP and literature XRD value, respectively), N1-C6-C5-C4 (50.8° (B3LYP), 54.81° (XRD)). The equatorial orientation of alkyl and aryl groups are identified by their bond angles N1-C2-C3-C7 (-177.5 (B3LYP) and -173.8° (lit. XRD) and C5-C4-C3-C7 (-177.8 (B3LYP) and 173.5° (lit. XRD)). For the picrate anion moiety, a loss of proton from the picric results in the lengthening of C(23)-O(32) bond with a distance of 1.263 Å [32]. In addition, C(23)-C(24) (1.455 Å) and C(23)-C(28) (1.452 Å) distances are both longer than the normal aromatic C-C values 1.4 Å [38] due to the loss of hydroxyl proton at O(1) leading to the conversion from the neutral to anionic state.

Natural bond orbital (NBO) analysis: NBO analysis provides an efficient method for the study of intra- and intermolecular bonding and charge transfer interactions and provides a convenient basis for investigative or molecular systems synergistic interactions [39,40]. The NBO atomic theory also deals with the hybridization of the atoms involved in the bond and lone pair orbitals. Second-order micro-disturbance theory from some electron donor orbital, acceptor orbital, and the interaction stabilization energy reported [41,42]. The unfilled bond orbit energies (ϵ_i and ϵ_j , diagonal) and the NBO Fock

TABLE-3
SELECTED BOND ANGLES (°) AND DIHEDRAL ANGLES (°) OF COMPOUNDS 1-3

Bond	Compound 1	Compound 2	Compound 3
C2-N1-C6	115.1	115.1	115.0
C3-C2-C11	119.1	119.1	119.4
N1-C2-C11	110.2	110.2	110.2
C2-C3-C7	112.9	112.8	113.0
C4-C3-C7	114.2	114.1	114.3
C5-C6-C17	115.9	116.0	116.4
N1-C6-C17	110.7	110.7	110.9
C24-C23-C28	112.6	112.5	112.5
C23-C24-C25	123.1	123.1	123.1
C23-C28-C27	124.0	124.0	124.1
O33-N29-O34	122.5	122.6	122.5
O38-N31-O37	124.2	124.2	124.0
O35-N30-C36	124.7	124.6	124.6
Dihedral angle (°)			
N1-C2-C3-C7	177.5	177.6	176.4
C5-C4-C3-C7	-177.8	-178.4	-177.0
N1-C2-C3-C4	-52.4	-52.4	-53.4
N1-C6-C5-C4	50.8	50.5	50.5
H1A-N1-C2-C3	179.4	179.5	179.9
H1B-N1-C2-C3	-70.3	-70.8	-69.1
H1A-N1-C6-C5	-178.8	-178.8	-178.8
H1B-N1-C6-C5	65.8	66.1	65.1
C11-C2-C3-C4	74.4	74.4	73.2
C17-C6-C5-C4	177.9	177.5	178.1

matrix element (F_{ij} , off-diagonal) are given by Weinhold and Landis [40], second order perturbative energy lowering, according to the filled bond orbit occupation (q_i). The interactions formed by the orbit are $\sigma(\text{O-N})$, $\sigma^*(\text{C-C})$, $\pi(\text{C-N})$, $\pi^*(\text{C-N})$, $\sigma(\text{C-C})$, $\pi^*(\text{C-C})$, $\sigma(\text{C-H})$, $\sigma^*(\text{C-H})$ bond orbit, which stabilizes the resulting structure of the ICT. This charge transfer ($\sigma \rightarrow \sigma^*$, $\pi \rightarrow \pi^*$, $\text{LP} \rightarrow \sigma^*$, $\text{LP} \rightarrow \pi^*$) induces the large linearity of molecule. The calculated values of E (2) are shown in Table-4. The strong inter-intermediate hyper-conjugative interaction of π electrons of C20-C22, C21-C23, C25-C27, C30-C31 distribute to $\pi^* \text{C21-C23}$, C20-C22, C32-C35 and C33-C37 of the ring as evident from Table-4.

The interesting intramolecular hyperconjugative interaction of π electrons in the π^* antibonding orbit of C20-C22 to C21-C23 and C25-C27 leads to the stabilizing energy of 20.13 and 20.18 kcal/mol. This results in the addition of LP (1) O7 NPO to $\pi^*(\text{C1-C2})$, (C1-C5), resulting in enormous stabilization energy of 21.30, 20.76 kcal/mol, respectively, as shown in Table-4. The lone pair LP (2) O62 bond is obtained with compound 2 of the important interactions with the anti-bonding orbital of $\pi^*(\text{N8-H44})$ distributed at the energy of 30.77 kJ/mol. The LP (1) O62 binding is coupled to anti-bonding orbital of $\pi^*(\text{N8-H44})$, which contributes to 16.44 kJ/mol of energy (Table-4).

Mulliken charges: The atomic charge is used to describe the processes of charge transfer in the electronegativity equation and in reactions [43,44]. Mulliken charge analysis of compounds 1-3 is calculated using the B3LYP theory measure with the base set of 6-31G(d,b). Mulliken atomic charges of compounds 1-3 are presented in Table-5. The levels of five carbon atomic charges of piperidone ring for compound 1 are 00.071 (C2) to, -0.335 (C3) \bar{e} , 0.446 (C4) \bar{e} , -0.118 (C5) \bar{e} and 00.044 (C6) \bar{e} as shown in Fig. 4. It is worth to note that C2, C3, C5

TABLE-4
SECOND ORDER PERTURBATION INTERACTIONS
OBTAINED FROM NBO CALCULATIONS OF COMPOUNDS 1-3

Type	Donor (i)	Acceptor (j)	E ² (kJ/mol)		
			1	2	3
$\pi-\pi^*$	C20-C22	C21-C23	20.13	19.94	18.20
$\pi-\pi^*$		C25-C27	20.18	17.96	19.22
$\pi-\pi^*$	C21-C23	C20-C22	19.73	19.47	19.84
$\pi-\pi^*$		C25-C27	21.03	20.79	17.21
$\pi-\pi^*$	C25-C27	C20-C22	19.91	23.38	19.89
$\pi-\pi^*$		C21-C23	18.90	18.99	20.63
$\pi-\pi^*$	C30-C31	C32-C35	19.97	20.29	17.13
$\pi-\pi^*$		C33-C37	19.94	18.14	16.81
$\pi-\pi^*$	C32-C35	C30-C31	20.11	19.45	19.31
$\pi-\pi^*$		C33-C37	21.46	21.01	17.37
$\pi-\pi^*$	C33-C37	C30-C31	20.11	23.44	20.04
$\pi-\pi^*$		C32-C35	18.75	19.14	17.33
$\sigma-\sigma^*$	N1-H1A	C2-C3	1.85	2.08	2.09
$\sigma-\sigma^*$	N1-H1A	C4-C5	2.13	1.25	1.26
$n-\sigma^*$	LP(1)N1	C2-H2	9.29	9.45	7.88
$n-\sigma^*$	LP (2) O7	C1-C2	21.30	21.75	21.45
$n-\sigma^*$		C1-C5	20.76	20.24	20.56
$n-\sigma^*$	LP (1) O33	C16-H16	0.37	0.17	0.28
$n-\sigma^*$	LP (2) O62	H6-N8	1.73	1.16	1.67
$n-\sigma^*$	LP (1) O62	N8-H44	0.08	16.44	15.93
$n-\pi^*$	LP (2) O62	N8-H44	0.15	30.77	4.67

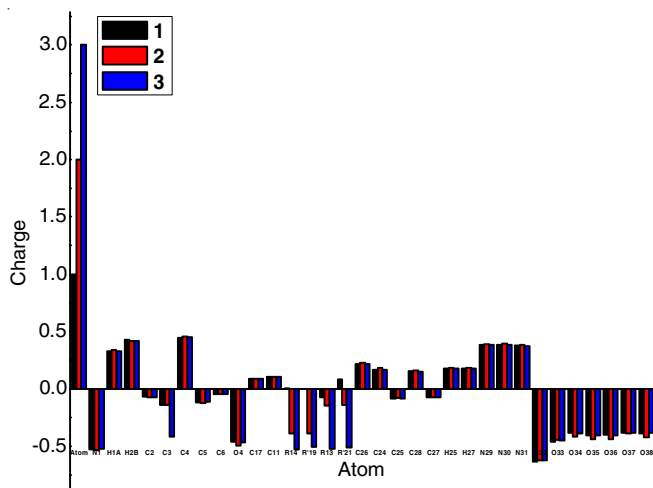


Fig. 4. Mulliken charge analysis of compounds 1-3

and C6 atoms of piperidone ring exhibit negative charges [45]. Mulliken population analysis revealed that N-1 and O32 atoms have the highest negative charge (0.528 and 0.638) in the

carbon atom (Table-5). Some carbon and hydrogen atoms have a maximum positive charge of H1A (0.327), C4 (0.446), N31 (0.377) and N30 (0.382).

Molecular electrostatic potential (MEP): Molecular electrostatic potential (MEP) simultaneously exhibits molecular shape, size and electrostatic potential in terms of colour classification. MEPs map has been found to be a very helpful tool in the analysis of molecular structures its relationship with the correlation physio-chemical property, including biomolecules and drugs [46]. The potential increases in the order red < yellow < green < light blue < blue. The negative electrostatic potential resembles the entirety of an atomic nucleus by proton of the electron density in molecule (shades of red) and the positive electrostatic potential of white matter (shades of blue and light green) [47]. The surfaces with red, yellow and blue colours represent negative, zero and positive values of energy, respectively. The MEP diagram for the current compound **1** is shown in Fig. 5 with the colour range from 00.0820 (deep red) to 0.143 (deep blue). In addition, the negative areas are actively located on the intermediate and intramolecular hydrogen bonded sides. Most of the hydrogen atoms of benzene are blue and pale green. The edge plot is a two-dimensional view of regions where the values of the corresponding electron density are within a certain range. In Fig. 5, N-H group shows a positive potential region of hydrogen atom over the surface (dark blue coloured/low electron density) [26].

Non-linear optical (NLO) analysis: Since the invention of laser, the NLO properties of organic molecules, especially those with strong D- π -A interaction have been extensively investigated in both experimental and theoretical studies and have been used extensively in optoelectronic and photonic devices [38,40]. All parameters [49] *i.e.* average polarizability (α_0), frequency-independent first-order hyperpolarizability (β), anisotropy of polarizability ($\Delta\alpha$), static dipole moment (μ), tensors and gas fraction of the investigated compounds 1-3 are given Tables 6 and 7.

The atoms in compounds 1-3 share electrons unequally. Due to this difference in electronegativity dipole moment arises. The dipole moment of compound **2** is considerably large difference shows in which high electronegativity of atoms bonded. Polarization composition of compound **2** represents the changes in electron cloud of the geometry [50]. The highest absolute value of dipole moment in z -direction is observed and the component μ_z value is equal to 13.7659. The calculated polarizability (α_{tot}) is equal to 8.85×10^{-24} esu. Thus μ_i and β_i for

TABLE-5
MULLIKEN ATOMIC CHARGES OF COMPOUNDS 1-3

Atom	1	2	3	Atom	1	2	3	Atom	1	2	3
N1	-0.528	-0.532	-0.524	R14	0.002	-0.388	-0.526	N29	0.381	0.392	0.384
H1A	0.327	0.342	0.329	R'19	-0.001	-0.387	-0.503	N30	0.382	0.393	0.381
H2B	0.425	0.417	0.417	R13	-0.079	-0.148	-0.521	N31	0.377	0.386	0.372
C2	-0.071	-0.075	-0.075	R'21	0.083	-0.144	-0.510	O32	-0.638	-0.624	-0.627
C3	-0.145	-0.144	-0.416	C26	0.216	0.227	0.215	O33	-0.461	-0.446	-0.450
C4	0.446	0.458	0.449	C24	0.168	0.181	0.167	O34	-0.385	-0.419	-0.391
C5	-0.118	-0.126	-0.115	C25	-0.086	-0.082	-0.090	O35	-0.404	-0.439	-0.406
C6	-0.044	-0.044	-0.046	C28	0.154	0.158	0.149	O36	-0.401	-0.437	-0.404
O4	-0.457	-0.495	-0.468	C27	-0.075	-0.074	-0.078	O37	-0.383	-0.390	-0.385
C17	0.090	0.089	0.087	H25	0.177	0.184	0.177	O38	-0.387	-0.423	-0.385
C11	0.104	0.104	0.104	H27	0.175	0.184	0.174	-	-	-	-

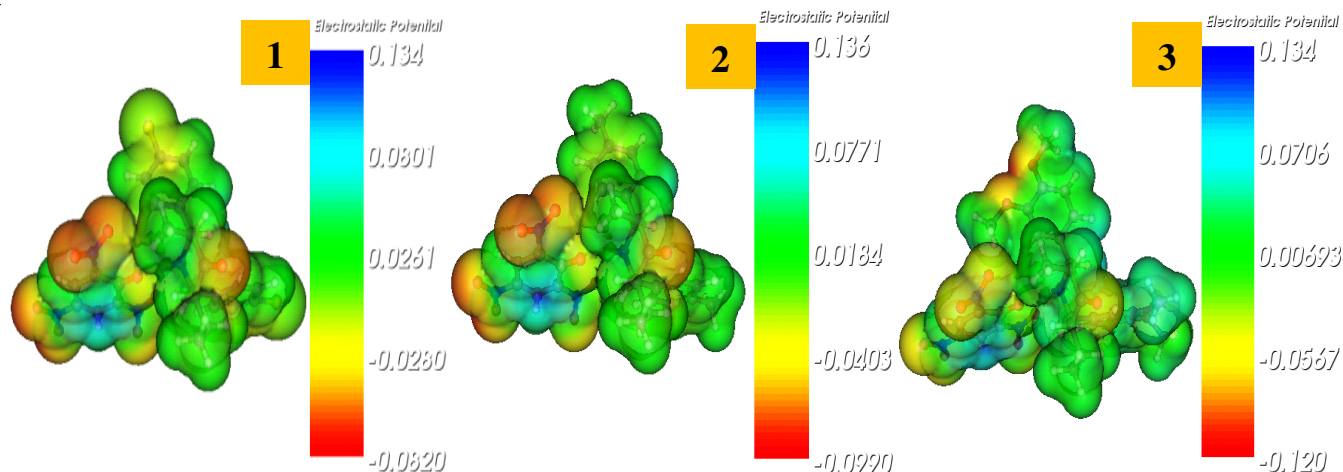


Fig. 5. Mapped electrostatic potential (MEP) of compounds 1-3

TABLE-6 DIPOLE MOMENT, POLARISABILITY OF COMPOUNDS 1-3			
Parameter	Compound 1	Compound 2	Compound 3
	Dipole moment (Debye)		
μ_x	8.895	12.904	11.056
μ_y	1.771	3.014	3.741
μ_z	0.316	-3.729	0.276
μ_{total}	9.075	13.766	11.675
Polarisability (a.u.)			
α_{xx}	291.22	271.43	293.71
α_{yy}	252.79	224.06	249.31
α_{zz}	258.75	243.69	286.02
α_{xy}	7.30	15.28	20.85
α_{xz}	3.27	15.86	1.36
α_{yz}	12.20	19.59	13.73
α_v (esu) $\times 10^{-23}$	3.97	3.65	4.1
$\Delta\alpha$ (esu) $\times 10^{-24}$	6.13	8.85	7.57

TABLE-7 HYPER POLARISABILITY VALUES OF COMPOUNDS 1-3			
Parameter	Compound 1	Compound 2	Compound 3
β_{xxx}	279.551	542.949	520.672
β_{yyy}	-19.887	93.223	189.527
β_{zzz}	-33.617	-52.369	-39.498
β_{xyy}	61.351	61.310	136.057
β_{xxv}	137.206	78.297	104.896
β_{xxz}	25.595	-64.493	44.211
β_{xzz}	5.957	22.326	47.834
β_{yzz}	-8.435	-5.311	27.599
β_{yyz}	43.479	-23.577	-17.373
β_{xyz}	41.160	71.536	58.332
β_0 (esu) $\times 10^{-30}$	3.16	5.73	6.69

compound 2 are 20 and 16 times that of corresponding values for urea. Hence, compound 2 is a strong candidate for the development of new NLO materials. The components of hyperpolarizability are useful to understand charge delocalization in the molecule. The maximum charge delocalization occurs along β_{xxx} in the molecule under investigation [51].

It can be seen from Table-7, first hyperpolarizability (α_{tot}) value of compound 3 is 6.69×10^{-31} esu, which is 15 times greater than the reference value [52]. The above results show that compound 3 is a very good material for NLO applications

[53]. The β value is more than that of urea value (6.69×10^{-31} e.s.u). Furthermore, due to the large b of present compound, it is assumed that the molecule has the potential to produce much larger than second-order optical effects with those got some other materials [50].

HOMO-LUMO analysis: By using HOMO and LUMO energy values for a molecule, the global chemical reactivity of molecule such as chemical electrophilicity index (ω), electronegativity (χ), softness (S), hardness (η) and chemical potential (μ) were defined [52,54]. Using Koopman's theorem [55] for closed-shell molecules. HOMO-LUMO gap Large molecules have a hard whereas, HOMO-LUMO gap molecules have a small soft. In terms of chemical reactivity, it is concluded that molecules such as reactive molecules will be hard for more than soft unimolecular isomerization and dissociation reactions. In the present study, ΔE_{H-L} gap value are reduced when 6-position of the molecule are substituted halogen [56]. The total energy, energy gap and electronegativity of a molecule stability. The frontier orbitals HOMO and LUMO are the most important parameters for the chemical reaction and chemical stability [57,58]. As a measure of electron conductivity, energy gap between the highest occupied molecular orbitals and the lowest unoccupied molecular is an important parameter in determining the electrical transport properties. The energy values of HOMO are computed -6.7484, -6.6444 and -5.9538 eV and LUMO are -2.9354, -2.8546 and -2.7681 eV, and the energy gap values are 3.813, 3.7898 and 3.1857 eV in the gas phase for compounds 1-3 as shown in Fig. 6 (Table-8). The π nature of HOMO is mainly located on phenyl ring and oxygen atom of picric acid. In contrast, the LUMO of picric acid is the only two nitro groups and consequently, the HOMO-LUMO transition implies the

TABLE-8 CALCULATED ENERGY VALUES (eV) OF COMPOUNDS 1-3 IN GAS PHASE			
B3LYP	Compound 1	Compound 2	Compound 3
E_{HOMO}	-6.7484	-6.6444	-5.9538
E_{LUMO}	-2.9354	-2.8546	-2.7681
$E_{LUMO-HOMO}$	3.813	3.7898	3.1857
Electronegativity	-4.8419	-4.7495	-4.3609
Hardness	1.9065	1.8949	1.5928
Electrophilicity index	6.148	5.952	5.9697
Softness	7.136	7.180	8.541

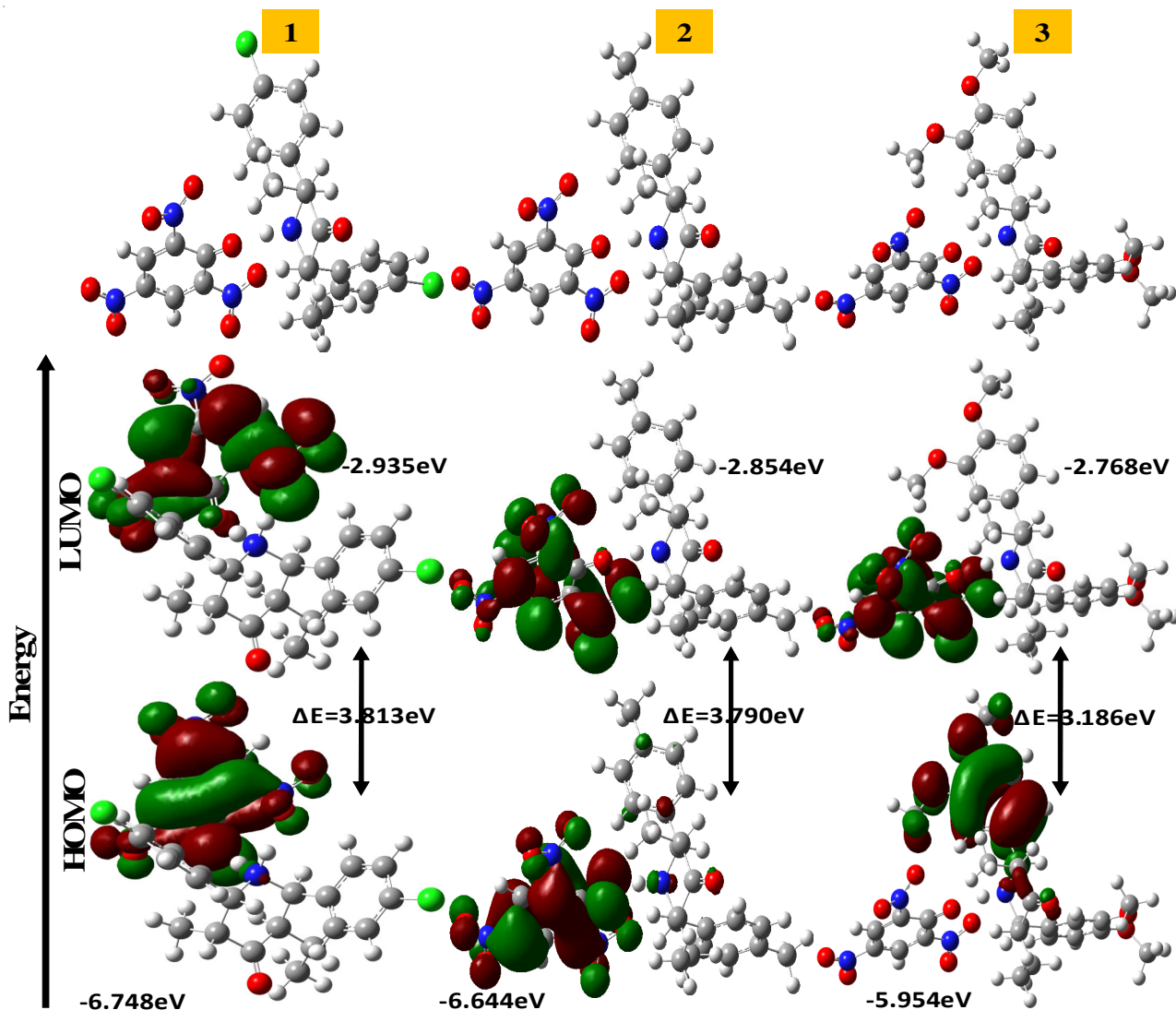


Fig. 6. Frontier orbitals of compounds 1-3 that have been computed by using B3LYP/6-31G level of theory

transfer of an electron density from phenyl ring to the two nitro groups and the lone pair of oxygen atom. This is a significant degree of charge transfer from electron-donor groups to intramolecular electron-acceptor groups [37].

Conclusion

Three picrate derivative compounds *viz.* 3-ethyl-5-methyl-2,6-*bis*(4-chlorophenyl)piperidin-1-ium picrate (**1**), 3-ethyl-5-methyl-2,6-*bis*(4-methylphenyl)piperidin-1-ium picrate (**2**), 3-ethyl-5-methyl-2,6-*bis*(3,4-dimethoxy phenyl)piperidin-1-ium picrate (**3**) have been synthesized and characterized. The fluorescence spectra revealed the three main emission and excitation peaks in the solid state at room temperature. The molecular geometry of ground state was calculated and compared with the experiment. Furthermore, first-order hyperpolarizabilities, total dipole moment, NBO and HOMO-LUMO energy gap have been calculated by using B3LYP methods with 6-31G (d,p) basis set in order to get an insight into the picrate compounds 1-3. The lower the HOMO and the LUMO energy gap (3.81), the better the total energy of the intramolecular interactions (20.76 kcal mol⁻¹) explain the eventual charge transfer interactions that take place within the molecules. The study of DFT

calculations and the first hyperpolarizability (α_{tot}) using weak interactions and non-linear optical properties in the molecule of energy is about 16 times that of urea.

CONFLICT OF INTEREST

The authors declare that there is no conflict of interests regarding the publication of this article.

REFERENCES

1. M. Arockia doss, S. Savithiri, G. Rajarajan, V. Thanikachalam and C. Anbuselvan, *Spectrochim. Acta A Mol. Biomol. Spectrosc.*, **151**, 773 (2015); <https://doi.org/10.1016/j.saa.2015.07.024>.
2. B. Roy, M.C. Reddy and P. Hazra, *Chem. Sci.*, **9**, 3592 (2018); <https://doi.org/10.1039/C8SC00143J>.
3. D. Rajaraman, G. Sundararajan, A. Kamaraj K. Krishnasamy and H. Saleem, *Spectrochim. Acta A Mol. Biomol. Spectrosc.*, **151**, 480 (2015); <https://doi.org/10.1016/j.saa.2015.06.037>.
4. D. Rajaraman, G. Sundararajan, R. Rajkumar, S. Bharanidharan and K. Krishnasamy, *J. Mol. Struct.*, **1108**, 698 (2016); <https://doi.org/10.1016/j.molstruc.2015.11.084>.
5. P.G. Farrell, F. Terrier and R. Schaal, *Tetrahedron Lett.*, **26**, 2435 (1985); [https://doi.org/10.1016/S0040-4039\(00\)94846-9](https://doi.org/10.1016/S0040-4039(00)94846-9).
6. G.C. Franchini, A. Marchetti, L. Tassi and G. Tosi, *J. Chem. Soc. Faraday Trans. I*, **84**, 4427 (1988); <https://doi.org/10.1039/F19888404427>.

7. B.I.M. Cooke, J.M. Diamond, A.D. Grinnell, S. Hgaiwara and H. Sakata, *Physiology*, **60**, 470 (1968).
8. N. Goel, U.P. Singh, G. Singh and P. Srivastava, *J. Mol. Struct.*, **1036**, 427 (2013); <https://doi.org/10.1016/j.molstruc.2012.12.020>.
9. M. Arockia doss, G. Rajarajan, V. Thanikachalam, S. Selvanayagam and B. Sridhar, *J. Mol. Struct.*, **1128**, 268 (2017); <https://doi.org/10.1016/j.molstruc.2016.08.065>.
10. H.I. El-Subbagh, SM. Abu Zaid, M.A. Mahran, F.A. Badira and A.M. Alobaid, *J. Med. Chem.*, **43**, 2915 (2000); <https://doi.org/10.1021/jm000038m>.
11. R.V. Perumal, M. Adiraj and P. Shanmugapandiyam, *Indian Drugs*, **38**, 156 (2001).
12. R.E. Hagenbach and H. Gysin, *Experientia*, **8**, 184 (1952); <https://doi.org/10.1007/BF02173735>.
13. A.R. Katritzky and W.J. Fan, *J. Org. Chem.*, **55**, 3205 (1990); <https://doi.org/10.1021/jo00297a041>.
14. C.R. Ganellin and R.G.W. Spickett, *J. Med. Chem.*, **8**, 619 (1965); <https://doi.org/10.1021/jm00329a015>.
15. S. Savithiri, M. Arockia doss, G. Rajarajan, V. Thanikachalam, H. Saleem and S. Bharanidharan, *Spectrochim. Acta A Mol. Biomol. Spectrosc.*, **136**, 782 (2015); <https://doi.org/10.1016/j.saa.2014.09.095>.
16. M. Arivazhagan and D.A. Rexalin, *Spectrochim. Acta A Mol. Biomol. Spectrosc.*, **107**, 347 (2013); <https://doi.org/10.1016/j.saa.2013.01.029>.
17. M.A. Asghar, J. Zhang, S. Han, Z. Sun, C. Ji, A. Zeb and J. Luo, *Chin. Chem. Lett.*, **29**, 285 (2018); <https://doi.org/10.1016/j.ccllet.2017.10.016>.
18. K. Tao, Z. Wu, S. Han, J. Zhang, C. Ji, Y. Wang, W. Zhang, J. Luo and Z. Sun, *J. Am. Chem. Soc.*, **6**, 4150 (2018); <https://doi.org/10.1039/C8TC00407B>.
19. T. Khan, M.A. Asghar, Z. Sun, C. Ji, L. Li, S. Zhao and J. Luo, *RSC Adv.*, **6**, 69546 (2016); <https://doi.org/10.1039/C6RA12178K>.
20. Y. Zhou, T. Chen, Z. Sun, S. Zhang, C. Ji, C. Song and J. Luo, *Chem. Asian J.*, **10**, 247 (2015); <https://doi.org/10.1002/asia.201402997>.
21. T. Dhanabal, G. Amirthaganesan, M. Dhandapani and S.K. Das, *J. Mol. Struct.*, **1035**, 483 (2013); <https://doi.org/10.1016/j.molstruc.2012.11.004>.
22. J. Jayabharathi, V. Thanikachalam, M. Venkatesh Perumal and N. Srinivasan, *J. Fluoresc.*, **22**, 409 (2012); <https://doi.org/10.1007/s10895-011-0974-4>.
23. S. Savithiri, M. Arockia doss, G. Rajarajan and V. Thanikachalam, *J. Mol. Struct.*, **1105**, 225 (2016); <https://doi.org/10.1016/j.molstruc.2015.10.063>.
24. T. Sun, W. Duan, Y. Wang, S. Hu, S. Wang, J. Chen and X. Shen, *J. Mol. Struct.*, **1148**, 206 (2017); <https://doi.org/10.1016/j.molstruc.2017.07.048>.
25. R.X. Li, L. Zhou, P.P. Shi, X. Zheng, J.X. Gao, Q. Ye and D.W. Fu, *New J. Chem.*, **43**, 154 (2019); <https://doi.org/10.1039/C8NJ03845G>.
26. M.J. Alam, A.U. Khan, M. Alam and S. Ahmad, *J. Mol. Struct.*, **1178**, 570 (2019); <https://doi.org/10.1016/j.molstruc.2018.10.063>.
27. H. Chermette, *J. Comput. Chem.*, **20**, 129 (1999); [https://doi.org/10.1002/\(SICI\)1096-987X\(19990115\)20:1<129::AID-JCC13>3.0.CO;2-A](https://doi.org/10.1002/(SICI)1096-987X(19990115)20:1<129::AID-JCC13>3.0.CO;2-A).
28. K. Ramirez-Balderrama, E. Orrantia-Borunda and N. Flores-Holguin, *J. Theor. Comput. Chem.*, **16**, 1750019 (2017); <https://doi.org/10.1142/S0219633617500195>.
29. L.H. Mendoza Huizar, C.H. Rios-Reyes, N.J. Olvera-Maturano, J. Robles and J.A. Rodriguez, *Open Chem.*, **13**, 1 (2015); <https://doi.org/10.1515/chem-2015-0008>.
30. E.D. Glendening, A.E. Reed, J.E. Carpenter and F. Weinhold, NBO Version 3.1, TCI, University of Wisconsin, Madison (1998).
31. F.S. Dukhovich and M.B. Darkhovskii, *J. Mol. Recognit.*, **16**, 191 (2003); <https://doi.org/10.1002/jmr.616>.
32. M.J. Frisch et al., Gaussian 03, Revision E.01, Gaussian Inc, Wallingford, CT (2004).
33. M. Arivazhagan and J. Senthil Kumar, *Spectrochim. Acta A Mol. Biomol. Spectrosc.*, **82**, 228 (2011); <https://doi.org/10.1016/j.saa.2011.07.040>.
34. Z. Demircioglu, F.A. Özdemir, O. Dayan, Z. Serbetçi and N. Özdemir, *J. Mol. Struct.*, **1161**, 122 (2018); <https://doi.org/10.1016/j.molstruc.2018.02.063>.
35. Y. Erdogdu, *Spectrochim. Acta A Mol. Biomol. Spectrosc.*, **106**, 25 (2013); <https://doi.org/10.1016/j.saa.2012.12.043>.
36. L. Li, T. Cai, Z. Wang, Z. Zhou, Y. Geng and T. Sun, *Spectrochim. Acta A Mol. Biomol. Spectrosc.*, **120**, 106 (2014); <https://doi.org/10.1016/j.saa.2013.10.011>.
37. S. Guidara, H. Feki and Y. Abid, *Spectrochim. Acta A Mol. Biomol. Spectrosc.*, **115**, 437 (2013); <https://doi.org/10.1016/j.saa.2013.06.080>.
38. M. Rajeshirke and N. Sekar, *Opt. Mater.*, **76**, 191 (2018); <https://doi.org/10.1016/j.optmat.2017.12.035>.
39. M. Kaur, Y. Sheena Mary, H.T. Varghese, C. Yohannan Panicker, H.S. Yathirajan, M.S. Siddegowda and C.V. Alsenoy, *Spectrochim. Acta A Mol. Biomol. Spectrosc.*, **98**, 91 (2012); <https://doi.org/10.1016/j.saa.2012.08.061>.
40. F. Weinhold and C.R. Landis, *Chem. Educ. Res. Pract. Eur.*, **2**, 91 (2001); <https://doi.org/10.1039/B1RP90011K>.
41. S. Subashchandrabose, A.R. Krishnan, H. Saleem, R. Parameswari, N. Sundaraganesan, V. Thanikachalam and G. Maikandan, *Spectrochim. Acta A Mol. Biomol. Spectrosc.*, **77**, 877 (2010); <https://doi.org/10.1016/j.saa.2010.08.023>.
42. C. James, A.A. Raj, R. Reghunathan, V.S. Jayakumar and I.H. Joe, *J. Raman Spectrosc.*, **37**, 1381 (2006); <https://doi.org/10.1002/jrs.1554>.
43. R.G. Parr and R.G. Pearson, *J. Am. Chem. Soc.*, **105**, 7512 (1983); <https://doi.org/10.1021/ja00364a005>.
44. R.S. Mulliken, *J. Chem. Phys.*, **23**, 1833 (1955); <https://doi.org/10.1063/1.1740588>.
45. N. Jeeva Jasmine, P. Thomas Muthiah, C. Arunagiri and A. Subashini, *Spectrochim. Acta A Mol. Biomol. Spectrosc.*, **144**, 215 (2015); <https://doi.org/10.1016/j.saa.2015.02.100>.
46. R. Shahidha, S. Muthu, M. Raja, R.R. Muhamed, B. Narayana, P.S. Nayak and B.K. Sarojini, *Optik*, **140**, 1127 (2017); <https://doi.org/10.1016/j.ijleo.2017.03.120>.
47. D. Ezhumalai, I. Mathivanan and A. Chinnadurai, *Spectrochim. Acta A Mol. Biomol. Spectrosc.*, **199**, 209 (2018); <https://doi.org/10.1016/j.saa.2018.03.053>.
48. A.J. Garza, O.I. Osman, A.M. Asiri and G.E. Scuseria, *J. Phys. Chem. B*, **119**, 1202 (2015); <https://doi.org/10.1021/jp507226v>.
49. M. Karabacak, L. Sinha, O. Prasad, Z. Cinar and M. Cinar, *Spectrochim. Acta A Mol. Biomol. Spectrosc.*, **93**, 33 (2012); <https://doi.org/10.1016/j.saa.2012.02.110>.
50. S. Aayisha, T.S. Renuga Devi, S. Janani, S. Muthu, M. Raja and S. Sevvanthi, *J. Mol. Struct.*, **1186**, 468 (2019); <https://doi.org/10.1016/j.molstruc.2019.03.056>.
51. K. Ramaiah, K. Srishailam, K. Laxma Reddy, B.V. Reddy and G. Ramana Rao, *J. Mol. Struct.*, **1184**, 405 (2019); <https://doi.org/10.1016/j.molstruc.2019.02.060>.
52. P.K. Chattaraj, B. Maiti and U. Sarkar, *J. Phys. Chem. A*, **107**, 4973 (2003); <https://doi.org/10.1021/jp034707u>.
53. E. Dhineshkumar, M. Iyappan and C. Anbuselvan, *J. Mol. Struct.*, **1177**, 545 (2019); <https://doi.org/10.1016/j.molstruc.2018.09.088>.
54. R.G. Parr, L.V. Szentpaly and S. Liu, *J. Am. Chem. Soc.*, **121**, 1922 (1999); <https://doi.org/10.1021/ja983494x>.
55. T.A. Koopmans, *Physica*, **1**, 104 (1934); [https://doi.org/10.1016/S0031-8914\(34\)90011-2](https://doi.org/10.1016/S0031-8914(34)90011-2).
56. Y. Erdogdu, S. Yurdakul, S. Badoglu and M.T. Güllüoğlu, *J. Mol. Struct.*, **1184**, 364 (2019); <https://doi.org/10.1016/j.molstruc.2019.02.016>.
57. R. Kumar, S. Obrai, J. Mitra and A. Sharma, *Spectrochim. Acta A Mol. Biomol. Spectrosc.*, **115**, 244 (2013); <https://doi.org/10.1016/j.saa.2013.06.021>.
58. K. Fukui, *Science*, **218**, 747 (1982); <https://doi.org/10.1126/science.218.4574.747>.